JOURNAL OF GEOPHYSICAL RESEARCH, VOL. 115, A03303, doi:10.1029/2009JA014327, 2010

IPY observations of ionospheric yearly variations from high- to middle-latitude incoherent scatter radars

Shun-Rong Zhang,[1] John M. Holt,[1] Anthony P. van Eyken,[2,3] Craig Heinselman,[4] and Mary McCready[4]

Received 2 April 2009; revised 16 October 2009; accepted 28 October 2009; published 9 March 2010.

[1] Upper atmospheric research during the 2007 International Polar Year features unprecedented yearlong observations by incoherent scatter radars. This valuable data set, collected under very low solar and magnetic activity conditions from a set of four radars spanning middle (Millstone Hill), auroral (Poker Flat), and higher latitudes (Sondrestrom and Svalbard), enables us to address a fundamental question of background climatology on ionospheric yearly variations. The main focus of this paper is on the noon-time baseline annual and semiannual variations, with an emphasis on the less-known height dependency, for those geophysically important areas. The radar measurements of ion drifts allow us to examine dynamic effects which have not been well addressed previously. High-latitude ionospheric climatology shows some interesting features, in particular, the two semiannual peaks of electron density N_e. The two peaks, neither of which is near summer solstice, are essentially of equinoctial symmetry at very high latitude sites, where downward ion drifts are strong in summer thus causing N_e reduction. The symmetry vanishes at the midlatitude site. Clear phase progression is seen from the topside to the $F2$ peak at the midlatitude site. Comparisons of Millstone Hill data from this period and prior solar minima indicate decreases in the ion temperature throughout the $F2$ peak and the topside ionosphere. These decreases do not seem to be associated with solar flux and magnetic activity effects.

Citation: Zhang, S.-R., J. M. Holt, A. P. van Eyken, C. Heinselman, and M. McCready (2010), IPY observations of ionospheric yearly variations from high- to middle-latitude incoherent scatter radars, *J. Geophys. Res.*, *115*, A03303, doi:10.1029/2009JA014327.

1. Introduction

[2] The International Polar Year (IPY) is a global scientific campaign dedicated to advancing our understanding of the Earth's polar regions. This current IPY covers a two year period of observations starting in March 2007 in a variety of science disciplines. A recent status and progress report is given by *Allison et al.* [2008]. The IPY upper atmospheric research featured unprecedented yearlong observations by a set of incoherent scatter radars (ISRs) at Svalbard (ESR, 78.1°N, 16.0°E), Poker Flat Incoherent Scatter Radar (PFISR, 65.1°N, 212.6°E), Sondrestrom (SDR, 67.0°N, 309.0°E), and Millstone Hill (MHR, 42.6°N, 288.5°E). It should be noted that ISRs' working schedule has traditionally been oriented toward short campaigns of a few days, and they have not been able to offer routine monitoring of the upper atmosphere mainly due to their high operational costs.

[3] This data set can be used to address some fundamental questions about upper atmosphere climatology, such as the yearly change of the ionosphere from high to middle latitudes, in particular the altitude dependency of such changes. Prior studies, largely based on the $F2$ peak density and total electron content (TEC) data as well as theoretical models, showed effects of two competing processes on middle- and low-latitude ionospheric annual and semiannual variations, i.e., solar zenith associated photoionization changes and general circulation and other processes associated neutral composition changes [*Torr and Torr*, 1973; *Fuller-Rowell et al.*, 1996; *Millward et al.*, 1996; *Rishbeth*, 1998; *Richards*, 2001; *Qian et al.*, 2009, and references therein]. Years of ISR observations at Shigaraki, a lower midlatitude site, were compiled to examine the yearly change, and it was indicated that seasonal anomaly in the electron density exists at altitudes near the ionospheric peak and below, but not quite so clear in the topside [*Balan et al.*, 1998; *Kawamura et al.*, 2002]. A series of ISR empirical models built upon long-term observations was also used to demonstrate some climatology of ionospheric annual and semiannual changes in a study by *Zhang et al.* [2005]. This current study, however, has some significantly different features from prior published results.

[1] MIT Haystack Observatory, Westford, Massachusetts, USA.
[2] EISCAT Association, Kiruna, Sweden.
[3] Now at SRI International, Menlo Park, California, USA.
[4] SRI International, Menlo Park, California, USA.

0148-0227/10/2009JA014327$09.00

[4] 1. Our observation was made during a single year period under rare conditions of the extended and deep low solar activity when magnetic activity was very low. Results from this study represent a background/baseline state of the upper atmosphere.

[5] 2. The unprecedented data sets have a high time resolution (from 2 weeks up to days) for annual/semiannual study, allowing for detecting more precisely features such as the phase change with height.

[6] 3. The simultaneous vertical drift measurements, as presented in the paper, provide information to understand the changing importance of the vertical dynamics over the year.

[7] 4. These observations by a set of four ISRs make comparisons of results for different latitudes more meaningful when background solar geophysical conditions were approximately the same.

[8] Also we found it interesting to compare current low solar activity observations with statistical results based on historical data from past solar cycles. The Millstone Hill ISR has generated a comprehensive data set spanning more than three solar cycles starting in the 1970s, and it will be used for our discussion. Therefore, this current study also features examination of changes in annual and semiannual variations over different solar cycles.

[9] This paper will report some new results of the high- and midlatitude ionospheric climatology obtained from these ISRs during the first year of the IPY, March 2007 through March 2008. In the following sections, we first describe solar geophysical conditions as well as observational and data processing details. Then we discuss results from annual and semiannual component decomposition for the 100–500 km height range and demonstrate clear midday semiannual peaks at high latitudes and pronounced phase progression from low to high altitudes at midlatitudes. Following these results, observations will also be compared with historical data at Millstone Hill to provide a qualitative view of changes over different solar cycles. The following section discusses some possible physical processes which may be responsible for the observed annual and semiannual changes. A summary section is provided to conclude this paper.

2. Observation and Data Processing

[10] March 2007 through March 2008 was a period of very low solar activity. The mean solar 10.7 cm flux (F10.7) was 72 solar flux units (s.f.u.) (1 s.f.u. = 10^{-22} W m^{-2} Hz^{-1}; hereafter F10.7 is treated as an index of s.f.u.) with a standard deviation of ±5 (or ~7% relative variability). Superposed on its regular 27 day periodicity, F10.7 increased a few times peaking at 94 on day 346 (12 December). The intervals between days 200 and 340 (later June solstice to December solstice) and between days 380 and 450 (mid January to the end of March 2008) were significantly less variable. The magnetic activity as represented by the daily *Ap* index was quiet as well: *Ap* has a mean value of 8 and a standard deviation of ±6. Although the standard deviation seems large, the variability is imposed on a very low level of magnetic activity. Figure 1 shows in the fifth and sixth panels the two indices with mean as well as high and low limits determined by standard deviations.

[11] ESR and PFISR were operating nearly continuously, and SDR and MHR were operating two days and one night twice per week. This means that we may address annual/semiannual variations at very high time resolution for ESR and PFISR sites; for SDR and MHR sites, changes beyond Nyqvist period of the data 28 days (compared to the typical 2 month Nyqvist period for most prior studies) are meaningful. In addition to these IPY regular observations, there were quite a few other experiments conducted by MHR and SDR during the period, and they have also been included in this study. These radars were normally making interleaved single pulse (SP) and alternating code (AC) measurements, with ESR doing the AC waveform only. This scheme generates an altitude resolution of a few kilometers for the *E* and lower *F* regions from the AC measurements, and a high signal-to-noise ratio but coarse height resolution of a few tens of kilometers for the *F* region and the topside from the SP measurements. The signal integration time was normally on the order of a few minutes. This study uses only the midday data within 30 min of local noon. At local noon, the magnetic local time is 1331 for ESR, 1315 for SDR, 1046 for AMISR, and 1226 for MHR. One of our primary interests is the vertical change; therefore, what is involved in this analysis is data from the fixed antenna (field-aligned directed) for ESR, the zenith antenna data for MHR, data with high elevation (>75°) for SDR, and data with a 77.5° elevation and −154.3° azimuth for PFISR, respectively.

[12] To compare the climatology from this IPY period with historical data, we also created a data set for MHR which contains all midday observations in the past three solar minima since the mid-1970s. We limit our data to days when F10.7 < 94, so that the mean F10.7 is 76 with a standard deviation of ±8 (mean *Ap* is 13 with a standard deviation of ±12), which is very comparable to the mean of 73 and standard deviation of ±7 obtained for the MHR observation conditions during the IPY period.

[13] Our focus is on the annual and semiannual components in the yearly variation; therefore, an annual and semiannual decomposition procedure is performed for each height bin. Although solar flux and geomagnetic variabilities were mostly small over the period, we take a simple first-order approach as explained by *Zhang et al.* [2005] and *Zhang and Holt* [2007] to account for their possible effects, i.e., $P = P_0 + P_1(f - \bar{f}) + P_2(a - \bar{a}) + P_3\cos(2\pi d/365 - d_1) + P_4\cos(4\pi d/365 - d_2)$, where P is either electron density N_e, ion temperature T_i, electron temperature T_e, or line-of-sight ion velocity V_0. The f is a combination of the daily 10.7 cm solar flux index F10.7 and corresponding 81 day average F10.7A, i.e., f = (F10.7 + F10.7A)/2, which has now been used in many upper atmospheric modeling studies [see *Richards et al.*, 1994; *Zhang and Holt*, 2007]. Here a is the 3 hourly *Ap* index, and $\bar{f}$ and $\bar{s}$ are the mean values of f and a for the data period (the first year's IPY). $P_{0,1,2,3,4}$ and $d_{1,2}$ are determined by singular value decomposition fitting. We take the same approach for the solar minimum data set from historical observations by MHR. Noting that (1) the two data sets correspond to similar solar-geophysical conditions as described earlier, and (2) we discuss only terms with solar flux and magnetic activity effects excluded as a first-order

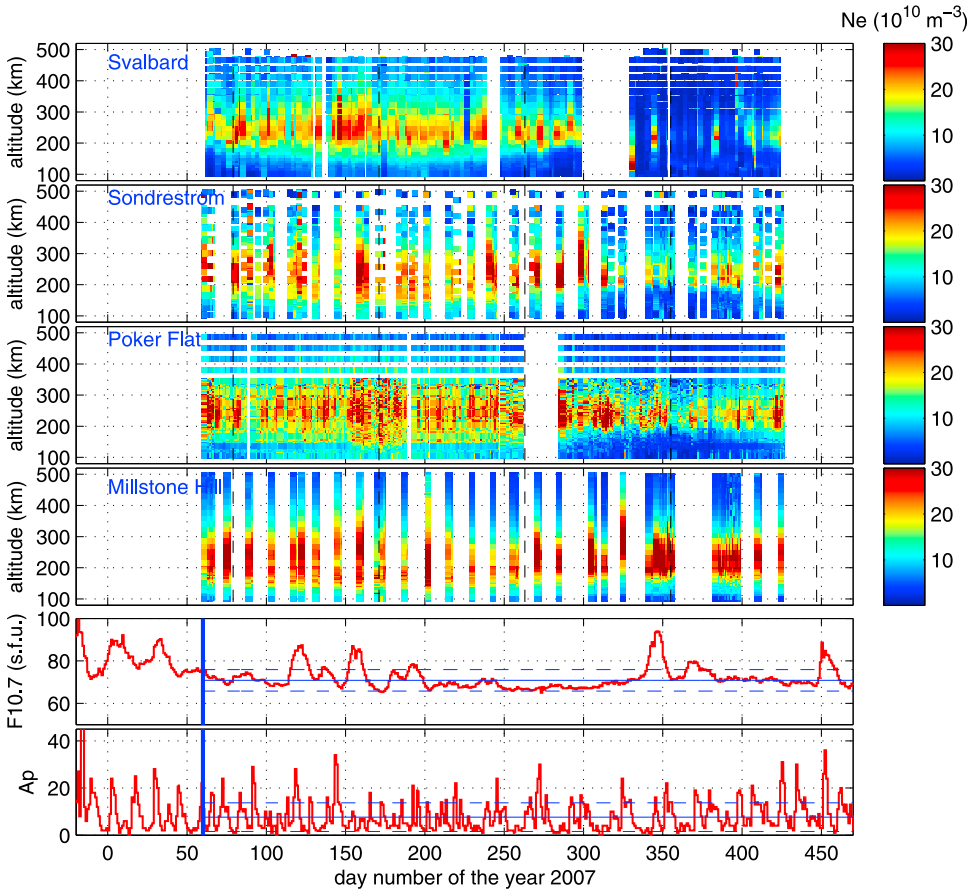

Figure 1. Observational midday electron density variations with height and day number over all the ISR sites considered in this study, along with solar geophysical indices of daily solar F10.7 flux and daily *Ap* during the first year of IPY. The black dashed lines indicate solstice and equinox days. The vertical blue lines indicate the start of the IPY observation. The horizontal blue lines in the geophysical index panels are mean (solid), and upper and lower limits (dashed) determined from standard deviation for daily F10.7 and *Ap* indices. The horizontal axis is the day number of the year 2007, with values over 365 for the first three months of 2008 and negative being for the year 2006.

approximation, we consider such comparisons between the IPY and historical data meaningful.

3. Results

3.1. Electron Density

[14] Original electron density data at midday are shown in Figure 1 for height versus day number variations over each of the four sites. The general feature of sharp winter–summer difference can be seen easily as a prominent annual variation; however, because of the solar flux effect, semiannual changes are less visible. The high flux around day 120, after day 150, and prior to day 350 corresponded well to the electron density enhancement above essentially all the four sites. During the quiet period between days 200 and 340 with a stable F10.7 level, ionospheric changes exhibit more likely the true and undisturbed seasonal trend, with an clear autumn peak in electron density above all sites. The above quick visual verification provides strong arguments for us to remove solar flux effects and perform annual and semiannual component decomposition, as suggested in the last section, in order to clearly identify background climatological changes. Now we present regression results for mean solar-geophysical conditions, i.e., annual and semiannual components only. Figure 2 shows height versus day number variations of the midday N_e.

[15] 1. At Svalbard, which has an invariant latitude of 76°, N_e exhibits a deep minimum in winter when the Sun is always set. The electron density N_e does not reach maximum in summer as would be expected from photochemical processes; instead, it has a weak minimum near summer solstice with higher densities midway between summer solstice and each of the two equinoxes. This situation is true near the *F*2 peak height (~230 km); with increasing height, these two separated peaks move closer toward summer and tend to merge; below the *F*2 peak region, the annual maximum is also close to summer solstice.

[16] 2. At Sondrestrom, with an invariant latitude of 74° similar to Svalbard, N_e is lowest in winter. The maximum density does not occur at summer solstice but very close to both equinoxes, with the autumn peak slightly higher than the spring one. In the bottomside of the *E* and lower *F* regions, a single annual maximum is present in summer. In the topside of above the *F*2 peak heights, the two peaks

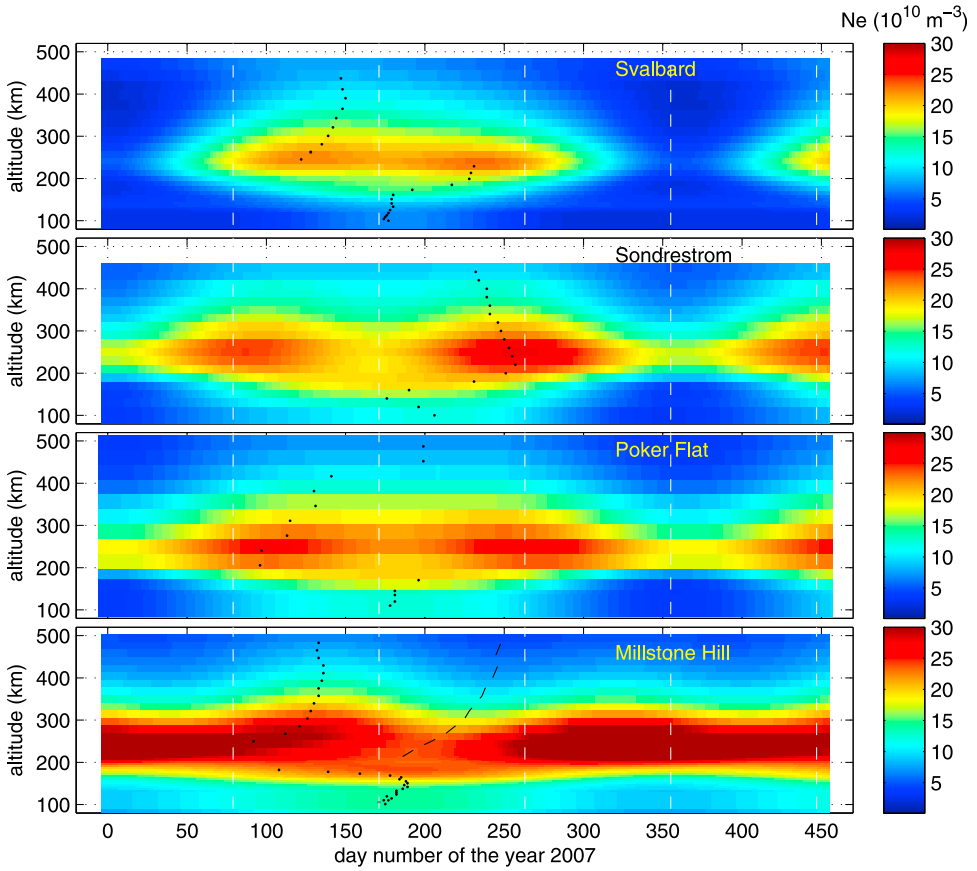

Figure 2. Electron density ($\times 10^{10}$ m^{-3}) variations as a function of day number and height for the four ISR sites, derived from a regression procedure based on the entire IPY data as discussed in the text. The results shown here are calculation for the IPY period and beyond. The horizontal axis is the day number of the year 2007, with values over 365 for the year 2008. The white dashed lines indicate solstice and equinox days. The phase of maximum (minimum) is determined as the day number of the maximum (minimum) N_e for the time period between spring and summer or between summer and autumn at a given height. Connecting these day numbers of maxima (minima, for Millstone Hill only) N_e at different heights forms the black dotted lines (dashed line).

are closer to each other toward summer than they are in the $F2$ peak region. Obviously, the situation for Sondrestrom is an intensified version of Svalbard in terms of the separation of pre- and after-summer peaks as well as the equinox over summer ratio of N_e, but the summer-over-winter ratio of N_e is in an opposite sense.

[17] 3. At Poker Flat, with an invariant latitude of 65°, N_e variations exhibit two peaks for the $F2$ region and an annual maximum in summer for the low altitudes. These characteristics are very similar to what is shown in SDR. The two equinox peaks are similar, and roughly speaking, symmetric to the summer solstice but more precisely symmetric to a slightly later time (by ~3 weeks) than the summer solstice. Although the so-called winter anomaly, here defined as the noontime N_e around the $F2$ peak being higher in winter than in summer [see *Rishbeth*, 1998; *Torr and Torr*, 1973, and references therein], does not show up, the noontime N_e in winter is obviously higher than at the higher-latitude sites.

[18] 4. Millstone Hill has an invariant latitude of 54°. Here the winter anomaly of midday N_e being higher in winter than in summer is a pronounced feature, which is absent for other higher-latitude sites. The highest N_e is in autumn-winter (November) for the $F2$ region, and in summer for the lower F and E regions. A secondary peak in the $F2$ region N_e is near spring equinox (April) varying with height. We also note the height change of the phase of the spring maximum and summer minimum. In Figure 2, the black dotted lines connect the days of maximum density at a given height during the spring and summer period or the summer and autumn period, and black dashed line (for Millstone Hill) the days of local minimum density at a given height during the summer and autumn period. From these maxima and minima, we can see the phase progression (delay) of electron density with height and day number. These time delays are an indication of chemical composition effects and plasma thermal dynamical effects which will be further discussed later.

3.2. Plasma Temperatures

[19] The solar irradiation provides the highest rate of solar heating in summer and the lowest in winter. Figure 3 shows some of the representative changes with clear seasonal variation patterns of T_i and T_e for these sites. T_e at MHR is

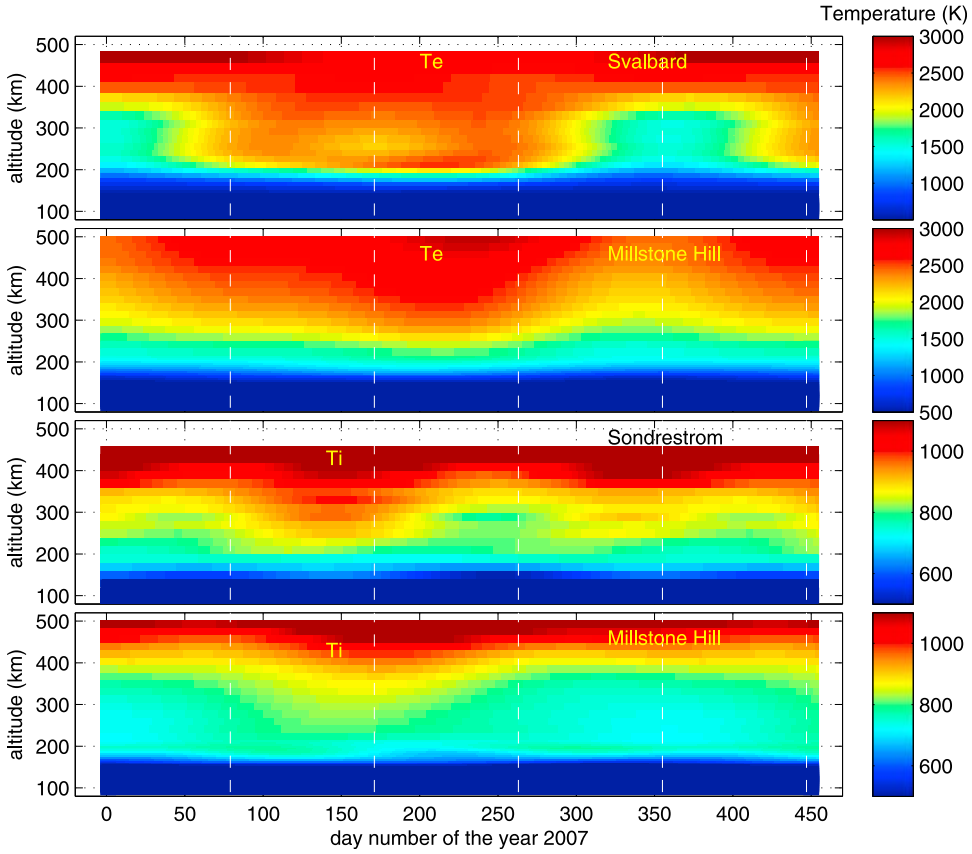

Figure 3. Same as Figure 2 but for variations of plasma temperatures. The first and second panels are T_e (K) for ESR and MHR, respectively; the third and fourth panels are T_i (K) for SDR and MHR, respectively.

highest in late summer. This timing is more or less consistent with that of N_e minimum, due to the well-known anticorrelation between T_e and N_e [see *Schunk and Nagy*, 1978; *Zhang et al.*, 2004]. The ESR T_e follows generally this yearly variation for MHR; however, there are some differences between the two sites: above 350 km T_e at Svalbard tends to be higher than at Millstone Hill, and below 350 km, T_e is smaller at Svalbard than at Millstone Hill. At Svalbard, T_e in the $F2$ peak height is enhanced slightly near the two equinoxes, but it is not the case for Millstone Hill where the annual maximum T_e occurs between the summer solstice and autumn equinox. The winter-summer difference in T_e at Millstone Hill is clearly less evident as at Svalbard.

[20] The ion temperature T_i carries important information about the neutral temperature at midlatitudes where T_i is very close to T_n from the E region up to the $F2$ peak (~250 km). Therefore, T_i in the $F2$ peak region and below is maximized at summer solstice for MHR (Figure 3), following the seasonal variation pattern of T_n. Below 350 km height, ESR T_i is higher in summer than in winter when it is the lowest among all sites for its highest geographic latitude (greatest solar zenith angle); SDR T_i variations (Figure 3) are more similar to MHR than ESR variations in terms of highest values around summer (below 350 km), implying a stronger control of solar EUV heating over other types of heating for such a site with 67°N geodetic latitude although in the very high magnetic latitudes. However, at auroral and higher latitudes, various heating processes have strong influences on T_i. Indeed, as shown in Figure 3, T_i is generally higher throughout the year at Sondrestrom than at Millstone Hill, and the annual peak T_i for Sondrestrom is not centered about the summer solstice but in later spring and early summer, while for Millstone Hill it is very close to the summer solstice.

3.3. Vertical Ion Drift

[21] The vertical ion drift affects electron density distribution through the chemical process of recombination which is strongly height dependent. In the $F2$ region, ambipolar diffusion along with the neutral wind-induced and electric field (such as the dynamo electric field) induced vertical ion motion is the main contributor of vertical ion drifts at high latitudes. The neutral wind, on the other hand, is also influenced strongly by the ion speed through the ion drag effects, which are seasonally dependent, and its phase also changes over a year.

[22] Unlike the horizontal drifts, $F2$ region vertical ion drifts at Sondrestrom are about the same order of magnitude as for Millstone Hill or even slightly larger and more vigorous compared with Millstone Hill. At Millstone Hill, the drift at midday is essentially downward below 300 km and upward above this height. As shown in Figure 4, in the 200–300 km range where the $F2$ peak density lies, the drift is more downward near equinox seasons, less downward in winter, and least downward in summer. The summer-to-winter circulation of the upper atmospheric wind system gives more

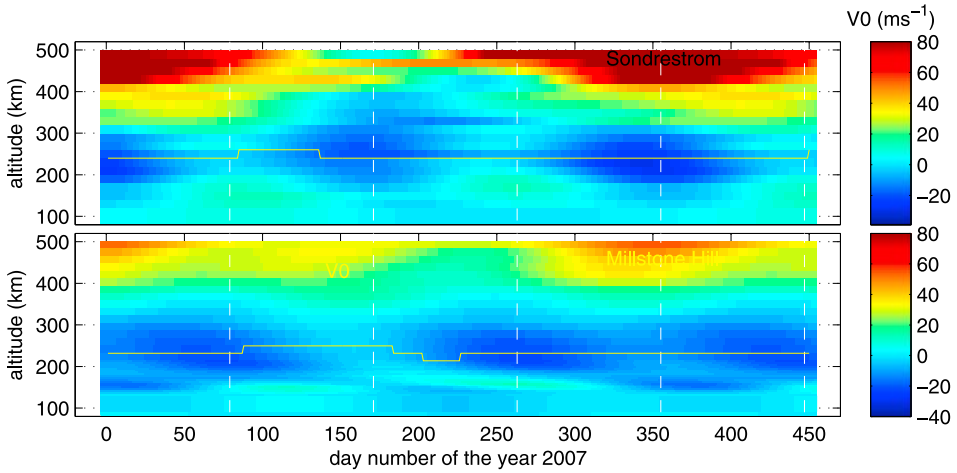

Figure 4. Same as Figure 2 but for variations of vertical ion drifts (m s^{-1}, positive for upward) as a function of day number and height for SDR and MHR. The yellow lines are the height of the *F*2 peak for N_e results shown in Figure 2.

equatorward meridional winds in summer; therefore, the wind-induced ion drift is more upward, leading to a reduced velocity of the overall downward ion drift. At Sondrestrom, the vertical drift is more downward in summer and winter than in equinox seasons. and the depletion of electron density in summer shown in Figure 2 is a very probable consequence of the drift. This will be further addressed later.

3.4. Comparisons Between IPY and Historical Data for MHR

[23] Important common features in N_e from comparing IPY data and those from previous solar minima (Figure 5) are (1) higher density in winter than in summer, (2) annual highest density in November–December, (3) secondary maximum density between spring equinox and summer solstice, and (4) the topside N_e variation exhibits a delayed phase to the peak region variation. The main difference lies in the stronger ionization in the F1 region shown in historical data. The F1 region is formed within 160–200 km heights where the linear ion–atom exchange rate (involving O^+) and the quadratic recombination rates (for the molecular ions) are close [*Rishbeth and Garriott*, 1969]. Whether this difference is due to changes in the EUV spectrum not reflected in F10.7 for the two cases is a question that needs more detailed study.

[24] The most interesting difference in T_i is the lower values in IPY than in previous solar minima. This temperature decrease occurs in the lower *F* region and prevails throughout the topside. It is height dependent, ranging from a few tens to ~100 K, but it becomes more significant with increasing height. Note that the mean year for the historical data taken at prior solar minima, which we are considering here, is approximately two solar cycles from this IPY period.

[25] As indicated in section 2, the two data samples for which comparisons are made have very similar geophysical conditions: F107 = 73 ± 7 (IPY data) versus 76 ± 8 (historical data); Ap = 8 ± 6 (IPY data) versus 13 ± 12 (historical data). There is a 3 s.u.f. difference in F107; differences in magnetic activity level and its variability are much larger. However, our IPY–historical data comparison is only for those regression results of background variations with solar flux and magnetic activity terms excluded; that is, the comparison of background variations is independent of solar flux and magnetic activity changes as a first-order approximation. Nevertheless, calculations with the empirical ISR model [*Zhang and Holt*, 2007], derived on the basis of long-term observations for Millstone Hill, indicate that each of the differences in F107 and *Ap* can only yield a small differences in T_i, ~10 K, and their combined effect is about ~20 K, which is well below the observed IPY-historical T_i differences discussed in the last paragraph (except for the very low heights). It seems unlikely that the observed differences are mostly due to contamination of solar flux and magnetic activity. Other possible causes of the temperature difference may be associated with solar-cycle variability [*Rishbeth and Field*, 1987], year-to-year variability, as well as the long-term trend of the upper atmosphere [*Roble and Dickinson*, 1989; *Emmert et al.*, 2004; *Holt and Zhang*, 2008], which is likely associated with the enhancement of greenhouse gas induced cooling at thermospheric and ionospheric altitudes (see *Lastovicka et al.* [2009] for more recent studies). These topics are beyond the scope of the paper but deserve some further study in future.

4. Discussion

4.1. Composition and Solar Flux

[26] We presented in Figure 2 very clear annual and semiannual components for the *F* region N_e above all these sites. The solar zenith angle χ annual changes and neutral composition ratio O/N_2 annual and semiannual variations [*Rishbeth*, 1998; *Qian et al.*, 2009; *Liu et al.*, 2007] can yield the two components. Figure 6 shows changes of $(O/N_2)\cos\chi$ for a fixed height of 250 km where O/N_2 is from the Mass Spectrometer Incoherent Scatter (MSIS) model [*Picone et al.*, 2002]. For MHR, the curve can be used to explain the winter anomaly and two equinox peaks due to the established fact that the *F*2 peak density at noon is closely related to the O/N_2 ratio. However, the severe semiannual asymmetry in N_e, being highest in November–December as

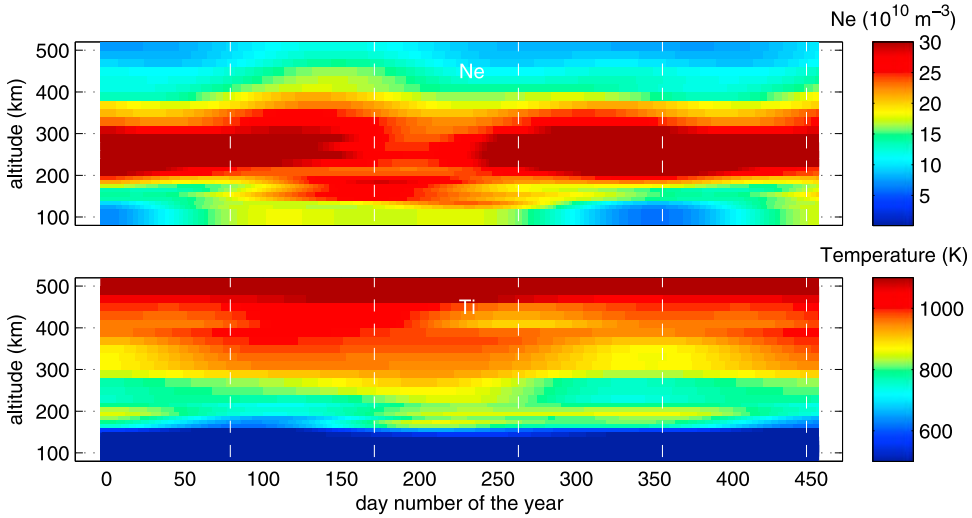

Figure 5. N_e ($\times 10^{10}$ m^{-3}) and T_i (K) variations as a function of day number and height for MHR obtained with historical data from prior three solar minima, with similar solar activity conditions to this IPY period. These are results derived from a regression procedure. Calculations for both cases are for day number 0–450, and the part after days 365 is the repetition.

shown in IPY and historical data, does not exist in the (O/N_2) $\cos\chi$ curve. This might be an indication that the MSIS gives less reliable semiannual asymmetry for O/N_2. In fact, CHAMP observations of the neutral density shown by *Liu et al.* [2007] indicated much higher density in spring than in autumn for low to middle latitudes at median solar activity. Therefore, it is likely that the true O/N_2 in autumn is higher than in spring. Direct observational evidence of the ratio over the IPY period is needed to examine this possibility.

4.2. Dynamic Effects and Time Delays

[27] From winter toward spring, the vertical ion drift becomes more downward moving the ions to regions of stronger chemical loss. Then effects of increasing (O/N_2) $\cos\chi$ toward spring, shown in Figure 6, on the $F2$ region N_e cancel those of increasing downward ion drifts; therefore, the spring N_e does not exceed the winter N_e. The spring N_e peaks about 1.5 months after the spring equinox (as well as the (O/N_2) $\cos\chi$ maximum time), and this is the time when the downward drift is turning to its summertime low level. When it goes from spring equinox to summer solstice, the $F2$ layer moves slightly up partially as a result of the reducing downward drift. The thick solid line in Figure 6 is the MHR result at 350 km for a comparison with 250 km results. Obviously, the (O/N_2) $\cos\chi$ height change does not cause the time delay in the topside N_e relative to the $F2$ peak as described earlier.

[28] There are other indications of dynamic processes modifying the annual variation, for instance, the different behavior of the topside and bottomside ionosphere and the phase changes (i.e., the time delay) between different heights as shown in Figure 2. These results of the phase change are meaningful, as it is larger than the time resolution of the original data. For the SDR and MHR cases where the time interval is about two weeks, although not as fine as days for ESR and PFISR, the phase changes by 1 month or longer over a 200 km height range from the $F2$ peak to the topside. The 1 monthlong delay is more likely associated with the increasing importance of plasma scale height effect, since the scale height increases with height above the $F2$ peak and from spring toward summer. Figure 7 demonstrates how the N_e profile shape changes from spring to summer when the corresponding plasma temperatures, which determine the scale height, increase. Results for autumn are also included for comparisons. The increase of the scale height from spring to summer can be seen in the topside N_e profile where N_e drops with height are much faster in equinox than in summer. This scale height increase is due to the increase in plasma temperatures, in particular T_e from 200 km to the topside (Figure 7). As a result, the N_e decrease toward summer is not as fast in the topside as in the $F2$ peak area. This slow decrease trend is found to be more significant with increasing height, since the plasma diffusion becomes more and more important with height than with the chemical effects. The time delay with height and season is therefore developed.

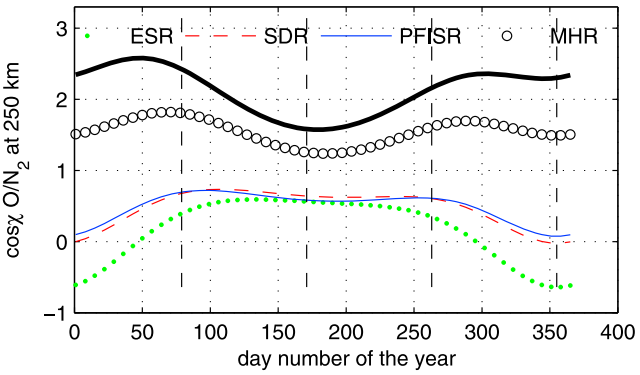

Figure 6. Yearly variations of midday $\cos\chi$ (O/N_2) at 250 km for the four ISR sites. The thick solid line is for MHR but at 350 km as scaled to one-third for better viewing. The vertical long dashed lines are days of spring equinox, summer solstice, autumn equinox, and winter solstice.

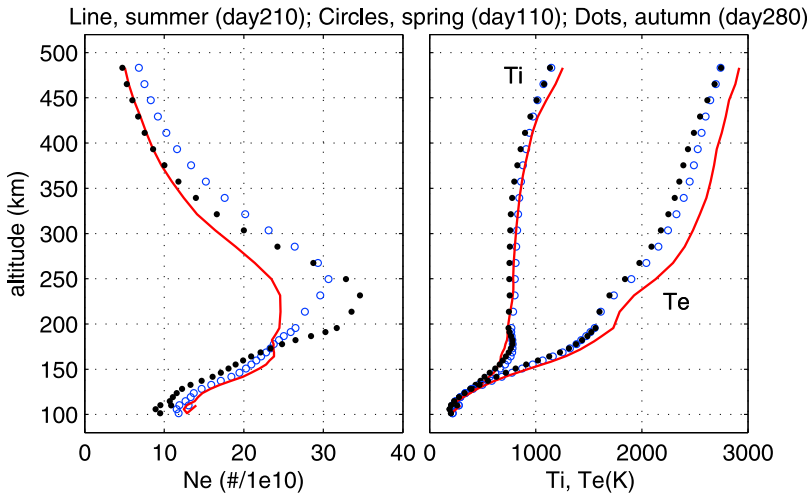

Figure 7. Millstone Hill height profiles of (left) N_e and (right) T_i and T_e for spring (circles), summer (line), and autumn (dots) to show effects of scale height changes with season.

[29] It is also interesting to note that the summer minimum N_e around the $F2$ peak is not exactly at summer solstice but about 1 month later. This may be associated with the time constant for the neutral atmosphere circulation effect to settle down. The $(O/N_2)\cos\chi$ curve does show some of this feature.

[30] The $(O/N_2)\cos\chi$ for PFISR and SDR is approximately the same, and N_e, behaving in a similar way for both sites, follows $(O/N_2)\cos\chi$ reasonably well. But the question is why the equinox peaks are so dominant over the summer density. The ratio results in Figure 6 are for a fixed height of 250 km. In fact, at SDR, the height of the $F2$ peak changes significantly over the year, being 30–40 km higher in spring and autumn than in summer. The vertical ion drift (Figure 4) is strongly downward (-40 m s^{-1}) in summer and clearly upward ($+20$ m s^{-1}) in the two equinoxes. Transport processes move the ions downward to regions of high chemical loss rates and account partially for the electron density depletion in summer at high latitudes.

4.3. Polar Cusp Location and Season Effects

[31] Both ESR and SDR are located at high latitudes with invariant latitudes of 74°–76°. It was indicated statistically [*Zhou et al.*, 2000] that the cusp's central latitude is 80.3° invariant latitude at noon, with a latitudinal width of 2°–3°. Therefore, there is a large possibility that some of our midday data were taken within the polar cusp where the ionosphere and thermosphere can be unique.

[32] There are seasonal changes in the polar cusp electron and ion precipitation which can result in corresponding ionospheric ionization changes. The summer cusp lies much closer to the sub-solar point where magnetosheath flow is more stagnated and low-energy ions can more easily enter the cusp, while the winter cusp is more toward the tailward and the magnetosheath flow is larger [*Newell and Meng*, 1988]. Such summer-winter difference in the dipole tilt angle tends to provide more ionizations in summer, less ionizations in winter, and moderate ionizations in equinox.

[33] The cusp location changes with solar wind conditions. It moves to a lower latitude for a larger southward interplanetary magnetic field (IMF) B_z, and the latitudinal width of the cusp is thicken for a larger solar wind dynamic pressure [*Zhou et al.*, 2000]. Figure 8 shows the yearly variations of IMF B_z and solar wind dynamic pressure. A 90 day running average is obtained in order to examine the seasonal change and possible modification to the high-latitude ionospheric variations (through changes of the cusp location, for instance) of the two parameters. Between days 250 and 350, B_z was more northward; therefore, the cusp was located likely more in the north in autumn than in other seasons. In Figure 2, however, N_e results for ESR and SDR do not seem to show direct influences of this type of annual changes in IMF B_z. The solar wind dynamic pressure was slightly low in the spring–summer period during its annual variation; however, N_e changes for the two sites do not seem to be correlated to it.

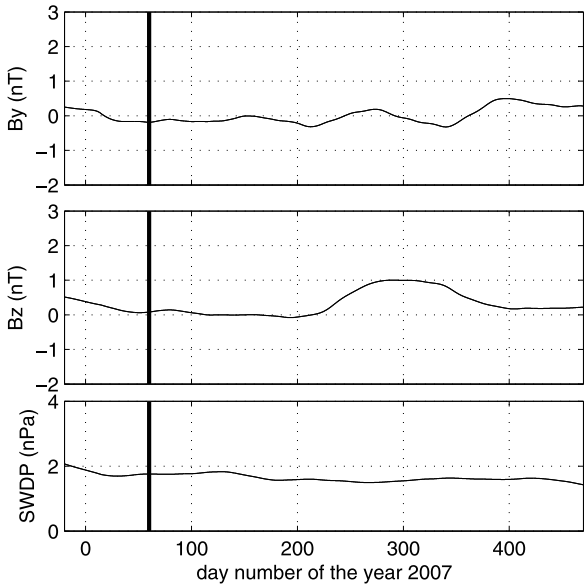

Figure 8. Yearly variations of 90 day running averages of IMF B_y and B_z GSM (nT) and solar wind dynamic pressure (nPa). The heavy vertical lines are the starting day of the IPY observation.

[34] For different IMF B_y values, ionospheric conditions can be very different at high latitudes; e.g., for the northern hemisphere, a positive B_y causes stronger dawnside convection, while an negative B_y causes stronger duskside convection (see *Zhang et al.* [2007, and references therein] for a recent study). During the IPY period, however, it is indicated in Figure 8 that there is only a weak fluctuation in the 90 day running averages of the IMF B_y, being slightly (<1 nT) more positive (north) in winter. But contributions from this weak seasonal asymmetry in B_y seems to be insignificant to the observed seasonal variation discussed here.

[35] Horizontal convection at high latitude is a well-known major process. Higher-electron-concentration plasma at lower latitudes (e.g., auroral latitudes) is dawn through the cusp into the polar cap. As a result of such horizontal transportation, electron density variations over these latitudes tend to be closely related or even similar. There are seasonal changes in the source of convecting plasma originated from lower latitudes. There exist also some seasonal changes in the convecting electric fields, with cross polar cap potential being slightly highly in equinox than in solstice [see *de la Beaujardiere et al.*, 1991; *Zhang et al.*, 2007], but these electrodynamic seasonal changes are perhaps secondary as compared to the substantial seasonal changes related to solar photoionization.

5. Summary

[36] This study addresses yearly ionospheric variations at noon using an unprecedented ISR data set from the first year's IPY observations at midlatitude, auroral, and higher-latitude locations. These observations made under very low solar and magnetic activity conditions help characterize the baseline annual and semiannual variations for those geophysically important areas. The radar measurements of ion drifts allow us to examine dynamic effects, which have not been well addressed previously while composition and solar radiation effects are better known. We have focused on the midday behavior as a function of height, and highlighted some important and unusual features embedded in the data. Detailed theoretical modeling is needed to explore fully the causes of these phenomena.

[37] Using an annual and semiannual component decomposition method, this study reveals some features of high-latitude ionospheric climatology. The electron density N_e for all the sites exhibits two peaks (a semiannual component) over the year and a winter minimum at high latitudes, but none of the sites show a peak near summer solstice. The two peaks are more or less semiannual symmetric with respect to the summer solstice at those high-latitude sites, but not midlatitude sites with N_e being higher for the second half of the year. The high-latitude sites present stronger downward ion drifts in summer than in other seasons, which may result in the summertime N_e reduction. The time delay of the topside variation with respect to the $F2$ peak region as seen at the midlatitude site may be caused by the changing importance of scale height effects with height and season.

[38] Comparisons of MHR T_i from this yearlong campaign and from historical data obtained in the last solar minima indicate qualitatively temperature decreases throughout the $F2$ peak and the topside ionosphere. These decreases do not seem to be associated with solar flux and magnetic activity effects.

[39] **Acknowledgments.** We thank the members of the MIT Haystack Observatory and of other ISR sites for maintaining the Madrigal Database. The Millstone Hill, Sondrestrom, and Poker Flat ISRs are supported by the U.S. NSF under Cooperative Agreements ATM-0733510, ATM-0334122, and ATM-0608577. EISCAT is an international association supported by the research councils of Finland (SA), France (CNRS), the Federal Republic of Germany (MPG), Japan (NIPR), Norway (NFR), Sweden (VR), the United Kingdom (PPARC), and China (CRIRP).

[40] Zuyin Pu thanks Alan Rodger and two other reviewers for their assistance in evaluating this paper.

References

Allison, I., M. Béland, and D. Carlson (2008), Status and progress of the International Polar Year, *Eos Trans. AGU*, *89*(34), 313, doi:10.1029/2008EO340001.

Balan, N., Y. Otsuka, S. Fukao, and G. J. Bailey (1998), Equinoctial asymmetries in the ionosphere and thermosphere observed by the MU radar, *J. Geophys. Res.*, *103*, 9481–9486.

de la Beaujardiere, O., D. Alcayde, J. Fontanari, and C. Leger (1991), Seasonal dependence of high-latitude electric fields, *J. Geophys. Res.*, *96*, 5723–5735.

Emmert, J. T., J. M. Picone, J. L. Lean, and S. H. Knowles (2004), Global change in the thermosphere: Compelling evidence of a secular decrease in density, *J. Geophys. Res.*, *109*, A02301, doi:10.1029/2003JA010176.

Fuller-Rowell, T. J., M. V. Codrescu, H. Rishbeth, R. J. Moffett, and S. Quegan (1996), On the seasonal response of the thermosphere and ionosphere to geomagnetic storms, *J. Geophys. Res.*, *101*, 2343–2353.

Holt, J. M., and S.-R. Zhang (2008), Long-term temperature trends in the ionosphere above Millstone Hill, *Geophys. Res. Lett.*, *35*, L05813, doi:10.1029/2007GL031148.

Kawamura, S., N. Balan, Y. Otsuka, and S. Fukao (2002), Annual and semiannual variations of the midlatitude ionosphere under low solar activity, *J. Geophys. Res.*, *107*(A8), 1166, doi:10.1029/2001JA000267.

Lastovicka, J., R. A. Akmaev, and J. T. Emmert (Eds.) (2009), Long-term changes and trends in the atmosphere-ionosphere system: 5th IAGA/ICMA/CAWSES workshop "Long Term Changes and Trends in the Atmosphere," *J. Atmos. Sol. Terr. Phys.*, *71*, 1511–1612.

Liu, H., H. Lühr, and S. Watanabe (2007), Climatology of the equatorial thermospheric mass density anomaly, *J. Geophys. Res.*, *112*, A05305, doi:10.1029/2006JA012199.

Millward, G. H., H. Rishbeth, T. J. Fuller-Rowell, A. D. Aylward, S. Quegan, and R. J. Moffett (1996), Ionospheric F2 layer seasonal and semiannual variations, *J. Geophys. Res.*, *101*, 5149–5156.

Newell, P. T., and C.-I. Meng (1988), Hemispherical asymmetry in cusp precipitation near solstices, *J. Geophys. Res.*, *93*, 2643–2648.

Picone, J. M., A. E. Hedin, D. P. Drob, and A. C. Aikin (2002), NRLMSISE-00 empirical model of the atmosphere: Statistical comparisons and scientific issues, *J. Geophys. Res.*, *107*(A12), 1468, doi:10.1029/2002JA009430.

Qian, L., S. C. Solomon, and T. J. Kane (2009), Seasonal variation of thermospheric density and composition, *J. Geophys. Res.*, *114*, A01312, doi:10.1029/2008JA013643.

Richards, P. G. (2001), Seasonal and solar cycle variations of the ionospheric peak electron density: Comparison of measurement and models, *J. Geophys. Res.*, *106*, 12,803–12,819.

Richards, P. G., D. G. Torr, B. W. Reinisch, R. R. Gamache, and P. J. Wilkinson (1994), F2 peak electron density at Millstone Hill and Hobart: Comparison of theory and measurement at solar maximum, *J. Geophys. Res.*, *99*, 15,005–15,016, doi:10.1029/94JA00863.

Rishbeth, H. (1998), How the thermospheric circulation affects the ionospheric F2-layer, *J. Atmos. Sol. Terr. Phys.*, *60*, 1385–1402.

Rishbeth, H., and P. R. Field (1987), Latitude and solar-cycle patterns in the response of the ionosphere F2-layer to geomagnetic activity, *Adv. Space Res.*, *20*, 1689–1692.

Rishbeth, H., and O. K. Garriott (1969), *Introduction to Ionospheric Physics*, Academic, New York.

Roble, R. G., and R. E. Dickinson (1989), How will changes in carbon-dioxide and methane modify the mean structure of the mesosphere and thermosphere, *Geophys. Res. Lett.*, *16*, 1441–1444.

Schunk, R. W., and A. F. Nagy (1978), Electron temperatures in the F region ionosphere: Theory and observations, *Rev. Geophys. Space Phys.*, *16*, 355–399.

Torr, M. R., and D. G. Torr (1973), The seasonal behaviour of the F2-layer of the ionosphere, *J. Atmos. Terr. Phys.*, *35*, 2237–2251.

Zhang, S.-R., and J. M. Holt (2007), Ionospheric climatology and variability from long-term and multiple incoherent scatter radar observations: Climatology in eastern American sector, *J. Geophys. Res.*, *12*, A06328, doi:10.1029/2006JA012206.

Zhang, S.-R., J. M. Holt, A. M. Zalucha, and C. Amory-Mazaudier (2004), Mid-latitude ionospheric plasma temperature climatology and empirical model based on Saint Santin incoherent scatter radar data from 1966–1987, *J. Geophys. Res.*, *109*, A11311, doi:10.1029/2004JA010709.

Zhang, S.-R., J. M. Holt, A. P. van Eyken, M. McCready, C. Amory-Mazaudier, S. Fukao, and M. Sulzer (2005), Ionospheric local model and climatology from long-term databases of multiple incoherent scatter radars, *Geophys. Res. Lett.*, *32*, L20102, doi:10.1029/2005GL023603.

Zhang, S.-R., J. M. Holt, and M. McReady (2007), High latitude convection model based on long-term incoherent scatter radar observations in North America, *J. Atmos. Sol. Terr. Phys.*, *69*, 1273–1291, doi:10.1016/j.jastp.2006.08.017.

Zhou, X. W., C. T. Russell, G. Le, S. A. Fuselier, and J. D. Scudder (2000), Solar wind control of the polar cusp at high latitude, *J. Geophys. Res.*, *105*, 245–251.

C. Heinselman, M. McCready, and A. P. van Eyken, SRI International, Menlo Park, CA 94025, USA. (craig.heinselman@sri.com; mary.mccready@sri.com; tony.van.eyken@eiscat.com)

J. M. Holt and S.-R. Zhang, MIT Haystack Observatory, Rt. 40, Westford, MA 01886, USA. (jmh@haystack.mit.edu; shunrong@haystack.mit.edu)